Crystal Structure of the IMP-1 Metallo β-Lactamase from *Pseudomonas aeruginosa* and Its Complex with a Mercaptocarboxylate Inhibitor: Binding Determinants of a Potent, Broad-Spectrum Inhibitor[†,‡]

Néstor O. Concha,*[,§] Cheryl A. Janson,[||] Pam Rowling,[||] Stewart Pearson,[⊥] Christy A. Cheever,[⊥] Brian P. Clarke,[#] Ceri Lewis,[||] Moreno Galleni,[@] Jean-Marie Frère,[@] David J. Payne,[⊥] John H. Bateson,[#] and Sherin S. Abdel-Meguid[§]

Departments of Structural Biology, Protein Biochemistry, Anti-Infectives, and Medicinal Chemistry, SmithKline Beecham Pharmaceuticals, 709 Swedeland Road, King of Prussia, Pennsylvania 19406, and Laboratoire d'Enzymologie & Centre d'Ingénierie des Protéines, Institut de Chimie, B6 Sart Tilman, Université de Liège, B-4000 Liège, Belgium

Received November 8, 1999; Revised Manuscript Received January 31, 2000

ABSTRACT: Metallo β-lactamase enzymes confer antibiotic resistance to bacteria by catalyzing the hydrolysis of β-lactam antibiotics. This relatively new form of resistance is spreading unchallenged as there is a current lack of potent and selective inhibitors of metallo β-lactamases. Reported here are the crystal structures of the native IMP-1 metallo β-lactamase from *Pseudomonas aeruginosa* and its complex with a mercaptocarboxylate inhibitor, 2-[5-(1-tetrazolylmethyl)thien-3-yl]-*N*-[2-(mercaptomethyl)-4-(phenylbutyrylglycine)]. The structures were determined by molecular replacement, and refined to 3.1 Å (native) and 2.0 Å (complex) resolution. Binding of the inhibitor in the active site induces a conformational change that results in closing of the flap and transforms the active site groove into a tunnel-shaped cavity enclosing 83% of the solvent accessible surface area of the inhibitor. The inhibitor binds in the active site through interactions with residues that are conserved among metallo β-lactamases; the inhibitor's carboxylate group interacts with Lys161, and the main chain amide nitrogen of Asn167. In the "oxyanion hole", the amide carbonyl oxygen of the inhibitor interacts through a water molecule with the side chain of Asn167, the inhibitor's thiolate bridges the two Zn(II) ions in the active site displacing the bridging water, and the phenylbutyryl side chain binds in a hydrophobic pocket (S1) at the base of the flap. The flap is displaced 2.9 Å compared to the unbound structure, allowing Trp28 to interact edge-to-face with the inhibitor's thiophene ring. The similarities between this inhibitor and the β-lactam substrates suggest a mode of substrate binding and the role of the conserved residues in the active site. It appears that the metallo β-lactamases bind their substrates by establishing a subset of binding interactions near the catalytic center with conserved characteristic chemical groups of the β-lactam substrates. These interactions are complemented by additional nonspecific binding between the more variable groups in the substrates and the flexible flap. This unique mode of binding of the mercaptocarboxylate inhibitor in the enzyme active site provides a binding model for metallo β-lactamase inhibition with utility for future drug design.

Bacterial resistance to the most common and potent antibiotics has been rising in recent years (*1*). Selective pressure in hospitals and infant- and child-care facilities is selecting pathogenic microorganisms carrying resistance genes. Resistance against antibiotics occurs through a variety of mechanisms, one of which is the production of β-lactamases (*2*, *3*). β-Lactamases catalyze the hydrolysis of the amide bond of the β-lactam ring to produce the corresponding β-amino acid devoid of antibacterial activity (*4*). Of the four structural classes of β-lactamases (*5*−*7*), classes A, C, and D catalyze the hydrolysis of β-lactams using a serine-dependent mechanism and proceeding through an acyl−enzyme intermediate (*8*−*10*). Class B enzymes, the metallo β-lactamases, require zinc, cobalt, cadmium, or manganese for catalysis (*11*, *12*) and hydrolyze most classes of β-lactams, including the broad-spectrum carbapenems (*13*, *14*). First discovered in *Bacillus cereus* (*12*), metallo β-lactamase activity has now been found in several pathogenic species of *Bacteroides* (*15*−*20*), *Pseudomonas* (*21*, *22*), *Stenotrophomonas* (*23*), *Aeromonas* (*24*), *Chryseobacterium* (*25*), *Serratia* (*26*), *Klebsiella* (*27*), and *Shigella* (*28*). Unlike the serine β-lactamases, metallo β-lactamases are not inhibited by the classic β-lactamase inhibitors clavulanic acid, sulbactam, and tazobactam, but

[†] Work by M.G. and J.-M.F. was funded in part by EU Grant ERB-FMRX-CT98-0232.

[‡] The atomic coordinates of the native and complex crystal structures have been deposited in the Protein Data Bank (accession codes 1DD6 and 1DDK, respectively).

* To whom correspondence should be addressed: Mail Code UE0447, 709 Swedeland Rd., King of Prussia, PA 19406. Telephone: (610) 270-7462. Fax: (610) 270-4091. E-mail: nestor_o_concha@sbphrd.com.

[§] Department of Structural Biology, SmithKline Beecham Pharmaceuticals.

[||] Department of Protein Biochemistry, SmithKline Beecham Pharmaceuticals.

[⊥] Department of Anti-Infectives, SmithKline Beecham Pharmaceuticals.

[#] Department of Medicinal Chemistry, SmithKline Beecham Pharmaceuticals.

[@] Université de Liège.

10.1021/bi992569m CCC: $19.00
Published on Web 03/25/2000

are inhibited by the metal chelators EDTA and *o*-phenanthroline (*29*). Thiol compounds such as mercaptophenyl acetate (*30*), *N*-(2′-mercaptoethyl)-2-phenylacetamide (*31*), or others (*32*) are competitive inhibitors and presumably bind through interactions between the inhibitor's thiolate and the active site metal(s). Recently, the crystal structures of the *Bacteroides fragilis* enzyme in complex with the buffer morpholinoethane sulfonate (MES) (*33*) and in complex with a biphenyl tetrazole inhibitor (*34*) have been reported. However, potent and selective inhibitors that are useful in the treatment of bacterial infections are yet to be reported. The increase in the β-lactam antibiotic resistance that parallels the production of metallo β-lactamases in pathogenic bacteria makes these enzymes an attractive target (*3*). One approach to overcoming this emerging resistance mechanism would be the design of a metallo β-lactamase inhibitor to be administered in combination with a β-lactam antibiotic. Inhibitors of these enzymes would consequently prolong the effective lifetime of conventional β-lactam antibiotics. Such inhibitors are particularly needed since the β-lactamase inhibitors that are currently used are completely ineffective against the metallo β-lactamases (*13*, *14*). The greatest progress toward potent, broad-spectrum, and selective metallo β-lactamase inhibitors has been reported (see the abstract of the American Society for Microbiology, General Meeting, May 30 to June 3, 1999, Chicago, IL) on a series of mercaptocarboxylate metallo β-lactamase inhibitors.

The crystal structures of the metallo β-lactamases from *B. cereus* (*35*, *36*) and *B. fragilis* (*33*, *34*, *37*, *38*) and the L1 from *Stenotrophomonas maltophilia* (*39*) show that the polypeptide chain adopts a fold consisting of four layers ($\alpha-\beta-\beta-\alpha$) with a central β-sandwich and two α-helices on either side. Located at one edge of the sandwich, the active site has either one or two Zn(II) ions (Zn1 and Zn2) separated by approximately 3.5 Å. In the crystal structures of metallo β-lactamases examined thus far, Zn1 is tetrahedrally coordinated to three histidines and a water molecule (shared between the metals). When present, Zn2 is coordinated to three residues (a cysteine, a histidine, and an aspartate) and two water molecules in a trigonal bipyramid as in *Pseudomonas aeruginosa*, *B. fragilis*, and *B. cereus*, or as in the L1 enzyme to an aspartate, two histidines, and two water molecules. The metal coordination geometry, the metal-to-metal distance, and the presence of the shared water are unchanged in the presence of MES (*33*) or the biphenyl tetrazole (*34*), both shown to be inhibitors of the *B. fragilis* enzyme. In the crystal structures of metallo β-lactamases that have a binuclear Zn(II) center, a water molecule (the shared water, also known as the bridging water, or hydroxide) coordinates to both metals. By analogy with other binuclear metal enzymes that have metal-bridging waters, the activation of the shared water, or hydroxide, provides the nucleophile for the reaction (*40*). Presumably, it is the addition of the hydroxide to the carbonyl carbon of the substrate that leads to the formation of a reaction intermediate that was independently observed by various investigators using spectroscopic methods. Their results suggest that a transient, noncovalent reaction intermediate is formed during the hydrolysis of the substrate nitrocefin catalyzed by the *B. cereus* (*41*), the L1 (*42*), and the *B. fragilis* (*43*) enzymes.

Analyses of the metal content of the enzymes from *Aeromonas* (*44*), L1 from *S. maltophilia* (*45*), *B. cereus* (*11*), and *B. fragilis* (*46*, *47*) indicate that these enzymes have retained the capacity to bind up to 2 mol of metal per mole of protein. In addition, the crystal structures and the amino acid sequence alignment [17−37% sequence identity (*37*)] indicate that these enzymes have all retained the binuclear metal binding motif. Functionally, however, they have different metal requirements, and can be divided into three subgroups. The *B. fragilis* and the L1 enzymes have two high-affinity metal binding sites that are required for catalysis (*46*). The *B. cereus* enzyme also has two metal binding sites; however, these metals bind with widely different affinities, 2.4 μM and 24 mM (*48*), and only the high-affinity site, Zn1, is required for near maximal enzymatic activity (*11*). Crystallization at different pHs has yielded crystal structures of the *B. cereus* enzyme with one (*35*) or two metals bound (*36*, *49*). The *Aeromonas* enzyme defines a third functional subgroup. It has one high-affinity zinc binding site (K_d < 20 nM), and binding of the second, low-affinity site inhibits the enzymatic activity with a K_i of 46 μM (*44*). This polymorphism in terms of the metal binding and its effect on the catalytic activity of the metallo β-lactamases may represent a rapidly evolving adaptive mechanism.

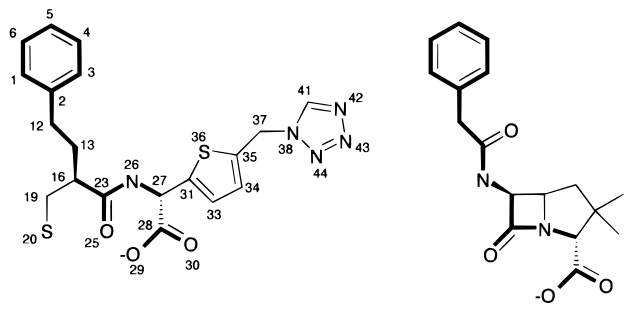

FIGURE 1: (Left) Structure of the mercaptocarboxylate inhibitor showing the atom numbering scheme. The stereochemical configuration that produces maximal inhibition of metallo β-lactamase activity is *S* at C16 and **D** at C27. (Right) Structure of benzylpenicillin. Bonds drawn with bold lines highlight the similarities between the mercaptocarboxylate inhibitor and the metallo β-lactamase substrate.

Imipenem resistance in clinical isolates of *P. aeruginosa* can be caused by two different mechanisms, either by reduced permeability combined with overproduction of a class C serine β-lactamase or by the production of the IMP-1 or VIM-1 metallo β-lactamase (*27*, *50*). The IMP-1 enzyme has been shown to be encoded by both plasmids and integrons (*51*), and these highly mobile genetic elements are thought to be responsible for the rapid spread of IMP-1 in clinical isolates from Japan. Recent data on the epidemiology of IMP-1 in Japan suggest that this metallo β-lactamase will probably be the most clinically significant of all the currently known metallo β-lactamases (*52*). Presented here is the crystal structure of the IMP-1 metallo β-lactamase from *P. aeruginosa* free and in complex with a mercaptocarboxylate inhibitor, 2-[5-(1-tetrazolylmethyl)thien-3-yl]-*N*-[2-(mercaptomethyl)-4-(phenylbutyrylglycine)] (Figure 1). The structural similarity between the β-lactams and this inhibitor and its interactions with conserved residues in the active site suggest the mode of binding used by the β-lactam substrates. The structure shows that three critical interactions provide selective inhibition against metallo β-lactamases: binding

into a hydrophobic pocket, interactions with a conserved lysine, and the metal ion interactions.

MATERIALS AND METHODS

Crystallization. The mature IMP-1 metallo β-lactamase from *P. aeruginosa* lacking the 18 amino-terminal residues that correspond to the signal sequence was overexpressed in *Escherichia coli* strain BL21(DE3) and purified as previously described (*53*). The soluble polypeptide includes 228 amino acid residues with a molecular weight of 25 000. Native crystals were obtained by vapor diffusion at room temperature (20−22 °C). They grew as thin plates (∼0.4 mm × ∼0.5 mm × ≤0.02 mm) after 2−3 weeks in 10 μL sitting drops equilibrated against 500 μL of reservoir solution. The drops were prepared by mixing 5 μL of protein [14 mg/mL in 20 mM HEPES (pH 7.5)] and 5 μL of reservoir solution containing 0.2 M sodium acetate, 30% PEG 4000, and 0.1 M sodium citrate buffer (pH 5.6) (the actual pH of the reservoir solution was 6.5). The crystals belong to space group $P2_1$ with unit cell dimensions $a = 50.3$ Å, $b = 105.8$ Å, $c = 112.3$ Å, and $\beta = 93.9°$, a tetramer in the asymmetric unit, and an estimated solvent content of 60%. The complex with the mercaptocarboxylate inhibitor, 2-[5-(1-tetrazolylmethyl)thien-3-yl]-*N*-[2-(mercaptomethyl)-4-(phenylbutyrylglycine)] (*30*, *53*), was prepared by mixing equal volumes of protein at a concentration of 14 mg/mL in 20 mM HEPES (pH 7.5) and to which an excess of solid inhibitor had been added with reservoir solution [30% PEG 2000 monomethyl ether, 0.1 M sodium acetate (pH 5.0), and 0.2 M ammonium sulfate]. This mixture was incubated overnight at 4 °C and centrifuged to remove precipitate before setting up crystallization drops. Cocrystals were grown from 6 μL sitting drops of the protein−reservoir solution and 0.3 mL of the reservoir solution at either room temperature or 4 °C. Crystals of the complex belong to space group $P2_12_12_1$ with unit cell dimensions $a = 50.0$ Å, $b = 51.6$ Å, and $c = 205.6$ Å, and have two copies of the IMP-1 metallo β-lactamase−inhibitor complex in the asymmetric unit.

Acquisition of X-ray Diffraction Data. Diffraction data to 3.1 Å resolution were obtained at room temperature from a single native crystal using a Siemens X-1000 multiwire area detector mounted on a Huber four-circle goniostat, and Cu Kα radiation produced by a Siemens rotating anode generator operating at 49 kV and 100 mA. The crystals were somewhat sensitive to the X-rays, and within the first several hours of data collection, the diffraction limit dropped from ∼2.8 to 3.1 Å. The reciprocal space was sampled at 0.25° intervals around the ω and ϕ axes, and the data were processed with XDS (*54*) (Table 1). Two diffraction data sets were measured from crystals of the complex with the mercaptocarboxylate inhibitor. The first set was measured at room temperature from two crystals using a MAR image plate. The reciprocal space was sampled in 0.75° oscillation steps around ϕ. These data were used for the structure determination and initial refinement. A second, higher-resolution set of data was collected at the NSLS X-25 beamline (Brookhaven National Laboratory, Upton, NY) from two flash-frozen crystals on a MAR345 detector using 1.100 Å wavelength X-rays. The crystals were cryoprotected by a brief exposure to the crystallization solution containing 20% glycerol. Data from the first crystal were collected in 0.75° oscillation steps, and data from the second crystal were collected in 1.0° steps. These crystals were not single, and data collection required a compromise between crystal-to-detector distance and oscillation range to avoid excessive overlap of the reflections. The data from the two crystals were integrated, merged, and scaled using DENZO/SCALEPACK (*55*) (Table 1).

Table 1: X-ray Data Collection and Structure Refinement

Data Collection Statistics	native	complex	
	I	I	II
unit cell dimensions	$a = 50.3$ Å $b = 105.8$ Å $c = 112.3$ Å $\beta = 93.9°$	$a = 50.1$ Å $b = 51.8$ Å $c = 206.0$ Å	$a = 49.3$ Å $b = 51.2$ Å $c = 203.3$ Å
space group	$P2_1$	$P2_12_12_1$	$P2_12_12_1$
no. of crystals	1	1	2
resolution (Å)	3.1	2.9	2.0
no. of observed reflections	31781	132605	545270
no. of unique reflections	19288	12384	34187
completeness (%)	90.1 (56.6)[a]	99.0 (99.9)[b]	95.9 (97.6)[c]
R_{sym}	0.140 (0.249)[a]	0.090 (0.286)[b]	0.103 (0.314)[c]

Refinement Statistics	native	complex
resolution (Å)	3.1	2.0
no. of reflections ($F > 2\sigma$)	19284	33694
no. of atoms (non-H)	1722	3878
R	0.260	0.198
R_{free}[d]	0.291	0.259
rms deviation from ideal		
bond lengths (Å)	0.007	0.018
bond angles (deg)	1.4	2.0
average *B* factors (Å^2)		
non-protein atoms	−	44
protein atoms	18	35

[a] The 3.19−3.10 Å resolution shell. [b] The 3.00−2.90 Å resolution shell. [c] The 2.07−2.00 Å resolution shell. [d] R_{free} was calculated with 10% of the reflections.

Structure Determination, Model Building, and Refinement. The crystal structure of the native IMP-1 metallo β-lactamase from *P. aeruginosa* was determined by molecular replacement (*56*, *57*) using reflections between 39 and 4 Å resolution and a Patterson search radius of 20 Å. The atomic coordinates of the metallo β-lactamase from *B. fragilis* (*37*) (PDB file 1ZNB) were used as the search model after the metals, solvent molecules, and atoms of residues that are not homologous were removed from the coordinate file. On the basis of the aligned amino acid sequences, 34% of the residues are identical in both enzymes (*37*). The solutions obtained from the rotation search corresponding to the four molecules in the asymmetric unit of the native crystal were the top four peaks with heights of 5.5−5.6σ (the next highest noise peak heights were 4.1σ and 3.8σ and lower) at $(\alpha_1,\beta_1,\gamma_1) = (76.41°, 113.93°, 138.25°)$, $(\alpha_2,\beta_2,\gamma_2) = (103.59°, 66.07°, 318.25°)$, $(\alpha_3,\beta_3,\gamma_3) = (256.51°, 114.83°, 138.51°)$, and $(\alpha_4,\beta_4,\gamma_4) = (283.49°, 65.17°, 318.58°)$. A Patterson correlation coefficient of 0.58 and a crystallographic *R* factor ($R = \Sigma_h||F_o| - |F_c||/\Sigma_h|F_o|$, where $|F_o|$ and $|F_c|$ are the observed and calculated structure factor amplitudes, respectively) of 0.48 were computed from the initial model that included the four molecules in the asymmetric unit. The structure of the complex was determined by molecular replacement using the partially refined native structure. The correlation coefficient and the crystallographic *R* factor

calculated from the initial model were 0.59 and 0.40, respectively. The program packages X-PLOR (*58*) and CNS (*59*) were used to refine the structures by rounds of simulated annealing and positional refinement followed by manual adjustment of the model with the aid of the interactive computer graphics program O (*60*). In the absence of a structure of the inhibitor, idealized versions of the molecule and its stereoisomers were built in QUANTA and energy minimized with CHARMM. The topology and parameter files used in the refinement were generated from the minimized structures (*61*). As a check of the correctness of the model structure, the stereoisomer that best fitted the electron density corresponded to the conformation that gave the highest inhibitory activity in the enzymatic assay. The convergence of the refinement was monitored by the fit of the polypeptide chain to the sigmaa-weighted (*62*, *63*) electron density maps calculated with coefficients $2|F_o| - |F_c|$ and $|F_o| - |F_c|$ and model phases, and by the value of the crystallographic *R* factor and R_{free} (*64*). All diffraction amplitudes to the limit of resolution were included with an allowance for the estimated bulk solvent contribution to the diffraction (*65*). Noncrystallographic symmetry restraints were imposed throughout the refinement except in the final rounds of refinement of the inhibitor complex in which the two molecules were refined independently (Table 1).

Enzyme Kinetics. The half-maximal inhibitory concentration, IC_{50}, was calculated as the concentration of inhibitor that caused a 50% reduction in the rate of hydrolysis of β-lactam substrate nitrocefin (*66*). The IC_{50} was determined following a preincubation of enzyme and inhibitor at 37 °C in 25 mM PIPES buffer (pH 7.0) with final Zn(II)SO_4 and nitrocefin concentrations of 100 and 400 μM, respectively.

RESULTS

Structure of the IMP-1 Metallo β-Lactamase. The crystal structure of the native IMP-1 metallo β-lactamase from *P. aeruginosa* was determined by molecular replacement, and the model was refined against data to 3.1 Å. The tetramer in the asymmetric unit has point group symmetry 222 (D_2), and each monomer includes residues 2−26 and 30−221 and two Zn(II) atoms. Residues 1, 27−29, and 222−228 are disordered and not included in the final model. The crystallographic *R* factor is 0.26; the R_{free} is 0.29, and the root-mean-square (rms) deviations from ideal bond lengths and bond angles (*67*) are 0.007 Å and 1.4°, respectively (Table 1). The structure of the complex between the IMP-1 metallo β-lactamase from *P. aeruginosa* and the mercaptocarboxylate inhibitor was also determined by molecular replacement, and the model refined to 2.0 Å resolution (Table 1 and Figure 2). The model consists of two molecules in the asymmetric unit, A and B, related by a rotation of 168.6°. Molecule A includes residues 4−223, two Zn(II) atoms, and one inhibitor; molecule B includes residues 4−225, two Zn(II) atoms, and an inhibitor. Residues 1−3 and 224− or 225−228 were disordered and are not included in the final model that in addition includes a total of 340 water molecules. The crystallographic *R* factor is 0.20; the R_{free} is 0.26, and the rms deviations from ideal bond lengths and bond angles (*67*) are 0.018 Å and 2.0°, respectively (Table 1). The average *B* factor is 27 $Å^2$ for molecule A and 43 $Å^2$ for molecule B, a difference that may reflect the number of crystal lattice contacts in which each molecule participates; 27 residues in molecule A establish direct protein−protein contacts with a symmetry-related molecule, with only 12 residues in molecule B. Superposition of the α-carbon atoms of the two independent molecules in the asymmetric unit gives an rms difference of 0.5 Å, with the largest differences being at both termini (2.6 Å difference) and between residues 22 and 31 (2.3 Å difference). When the residues with the largest differences are omitted, the resulting rms is 0.3. Residues 22−31 form two antiparallel β-strand segments, and the connecting turn is termed the flap. These residues participate in crystal lattice contacts between molecules A and B; residues 28−32 in molecule B contact residues 23−30 in molecule A such that the polypeptide chains are perpendicular to each other. Partly as a result of these interactions, the flap in molecule A is positioned between the active site-bound inhibitor and molecule B.

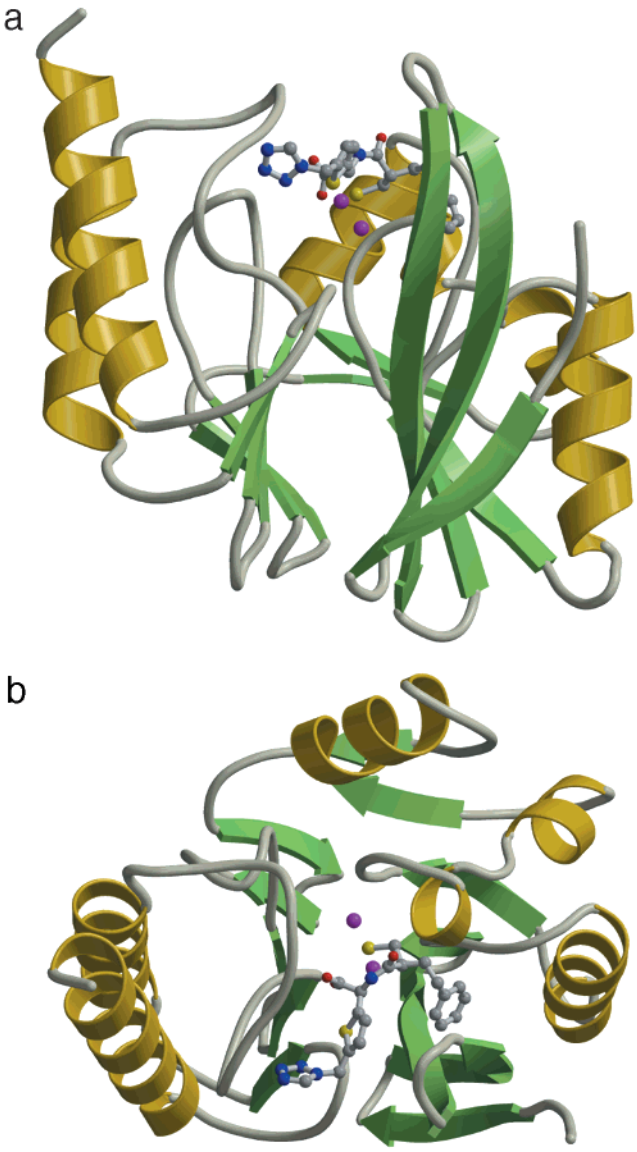

FIGURE 2: Secondary structure elements of the IMP-1 metallo β-lactamase from *P. aeruginosa* (*71*) in complex with a mercaptocarboxylate inhibitor. β-Strands are colored green. α-Helices are colored gold. The inhibitor is represented as a ball-and-stick model (nitrogen, blue; carbon, gray; oxygen, red; and sulfur, yellow). Zinc ions are represented as magenta spheres (*72*−*74*). (a) The mercaptocarboxylate inhibitor is bound in the active site at one edge of the central β-sandwich. (b) View of the structure after a 90° rotation about the horizontal axis of the view in panel a.

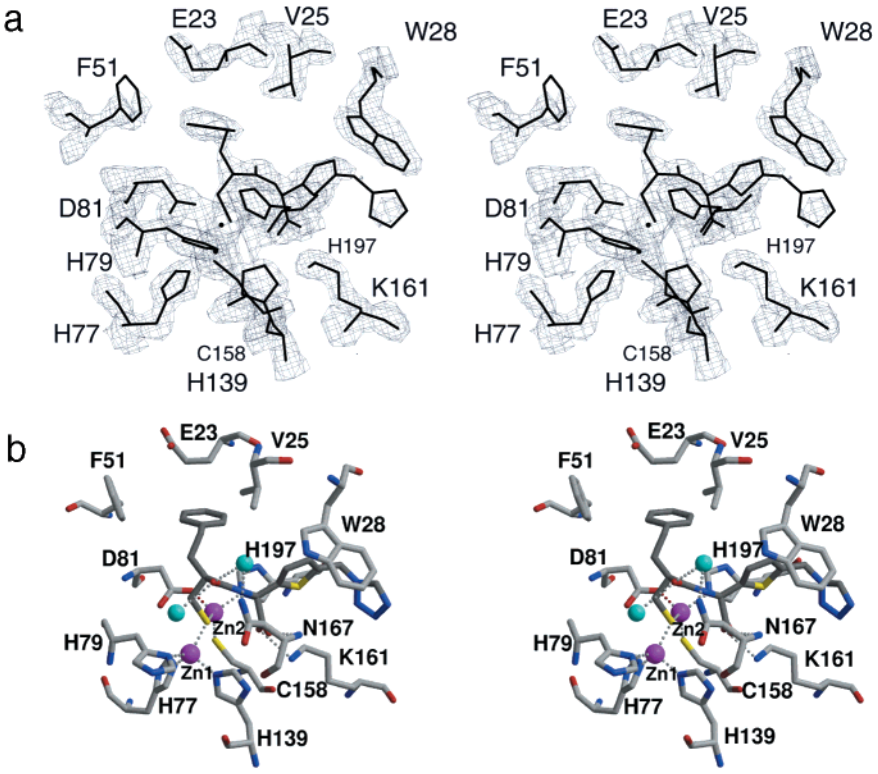

FIGURE 3: Binding of the mercaptocarboxylate inhibitor to the active site of the IMP-1 metallo β-lactamase from *P. aeruginosa*. (a) Sigmaa-weighted $|F_o| - |F_c|$ electron density map contoured at the 1.5σ level using phases calculated from the model in which the inhibitor, metals, and amino acid residues in the active site were omitted (*75*). (b) The inhibitor bonds are colored dark gray. The sulfur atom of the inhibitor that has displaced the bridging water bridges the zinc ions (magenta spheres). Trp28 is part of the closed flap and interacts with the thiophene ring of the inhibitor. The phenyl group of the inhibitor is bound to the hydrophobic pocket formed by Phe51, Val25, and Val31. Two water molecules (light-blue spheres) are bound to Asn167 and the carbonyl oxygen of the inhibitor. Dotted lines indicate polar interactions (*72*−*74*).

The rms difference for the superposition of the α-carbon atoms of the native and complex structures is 0.7 Å with the largest differences (3.5 Å) at the termini and the flap regions; when residues 4, 21−32, and 219 are omitted from the comparison, the rms deviation is 0.4 Å. In addition, the side chain of Phe51 shows a large difference in the position of the phenyl ring between the native and the complex. A rotation of 100° about the Cα−Cβ bond moves the phenyl side chain away from the S1 hydrophobic pocket to provide access to the inhibitor's phenyl group which binds at this site (Figures 3 and 6). The distance between the two Zn^{2+} atoms in the active site is 3.6 Å in the inhibitor complex and 3.5 Å in the native structure, a small difference well within the experimental error considering that the bridging water in the native structure (not seen at the resolution of 3.1 Å, but presumed present) was replaced by the sulfur atom of the inhibitor's thiolate (Figures 3 and 4). As in all known crystal structures of metallo β-lactamases, Asp48 has a sterically strained main chain conformation in both the native form and the complex with mean ϕ and ψ angles of 81° and 148°, respectively. The carboxylate oxygen atoms of Asp48 in the IMP-1 metallo β-lactamase make hydrogen bond and/or electrostatic interactions near the active site with Lys33 NZ (2.8 Å) (Figure 7b). Other interactions of Asp48 are with Ser82 OG (2.7 Å), Ser76 OG (2.8 Å), and Ser76 N (2.8 Å).

Binding of the Inhibitor. The mercaptocarboxylate inhibitor, with a half-maximal inhibitory concentration for nitrocefin hydrolysis of 90 nM, is bound in the active site of IMP-1 through electrostatic and nonpolar interactions. The stereochemical conformation that results in maximal inhibition of metallo β-lactamase activity is *S* at C16 and **D** at C27. Most of the interactions occur between the mercaptomethyl phenylbutyryl glycine portion of the inhibitor and the metals and conserved residues in the active site (Figure

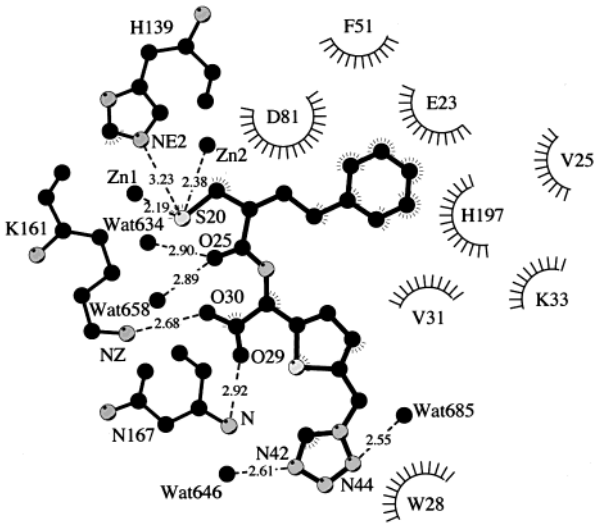

FIGURE 4: Diagram of interactions between the inhibitor and the metallo β-lactamase (*76*). Hydrogen bonds and electrostatic interactions are shown as dashed lines with the respective interatomic distances quoted; line segments radiating from the atoms indicate van der Waals contacts with atom(s) in the labeled residues surrounded by a sector with rays that show the direction of the interaction. Carbon atoms are represented as black spheres; oxygen, nitrogen, and sulfur atoms are represented as spheres with decreasing shades of gray.

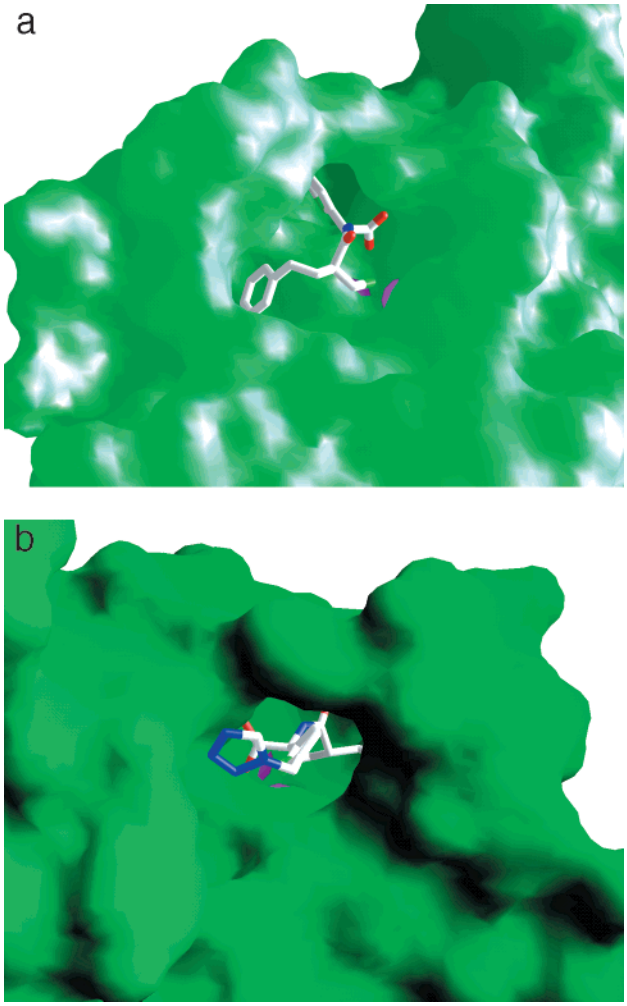

FIGURE 5: Molecular surface representation (*77*) of the IMP-1 metallo β-lactamase inhibitor complex. In the complex, the flap is closed over the mercaptocarboxylate inhibitor bound in the active site. (a) Front view of the bound inhibitor and its interaction with the Zn^{2+} (magenta) and the S1 hydrophobic pocket. (b) View from the opening of the active site tunnel distal to the metal center with the exposed tetrazole ring of the mercaptocarboxylate inhibitor.

4); the inhibitor's thiolate bridges the two Zn^{2+} atoms replacing the shared water, and the inhibitor's carboxyl group interacts with the side chain of Lys161 (2.8 Å) and the main chain amide nitrogen of Asn167 (2.9 Å). The carboxylate oxygen of the inhibitor is located 3.6 Å from Zn2, and has displaced the apical water from Zn2 which in the complex is coordinated to four ligands with a tetrahedral coordination geometry (Table 2). In molecule A, the inhibitor's carbonyl oxygen interacts with Wat135 (2.7 Å) and Wat160 (3.0 Å), and the latter also contacts Asn167 ND2 (2.8 Å). The carbonyl oxygen is exposed to solvent and oriented to establish interactions with but is distant from Zn1 (5.0 Å) and Asn167 ND2 (4.1 Å), both of which are proposed to form the oxyanion hole (*37*). Of the possible 675 $Å^2$ of solvent accessible area in the free inhibitor, only 99 $Å^2$ is exposed to solvent in the complex (Figure 5). Of these, 55 $Å^2$ corresponds to the tetrazole ring, and the remaining exposed surface is contributed by the carbonyl oxygen (15 $Å^2$), C12 (11 $Å^2$), C13 (15 $Å^2$), and C19 (3 $Å^2$).

The inhibitor's phenyl ring is bound in a hydrophobic pocket formed by residues Glu23, Val25, Val31, Lys33, and Phe51, next to the flap and near the metal center. Comparison with the native, unbound structure indicates that binding of the inhibitor requires a rotation of 100° about the Cα−Cβ bond of Phe51 to provide access to the hydrophobic pocket. In addition to or at the same time as this rotation, a displacement of 2.9 Å of the polypeptide at Val25 widens the pocket, and causes the lateral movement of the flap (Figure 6).

In the inhibitor complex, the flap is in the closed conformation, and the side chain of Trp28 interacts edge-to-face with the inhibitor's thiophene ring. The two molecules in the asymmetric unit provide slightly different views of the flap that vary in the degree of closure due to crystal lattice contacts. The conformation of the flap in molecule B is more open; its residues, 22−31, have higher *B* factors than in molecule A (58 and 39 $Å^2$, respectively), and the α-carbon positions of Trp28 differ by 2.2 Å between the two molecules. The inhibitor also shows differences between the two independent molecules. The inhibitor atoms bound to molecules A and B superimpose with an rms deviation of 0.7 Å with the largest differences between the thiophene and tetrazole groups at S36 (1.4 Å), C41 (1.5 Å), N44 (1.1 Å), and N42 (1.4 Å). When the atoms in these groups are excluded from the superposition, the mercaptomethyl phenylbutyryl glycine moiety superimposes with an rms deviation of 0.2 Å and binds in the same way to both molecules. Away from the metal center is where the conformation of the inhibitor differs most between the two molecules. In molecule A, the thiophene ring penetrates deep into the active site and is flanked by Val31 and Trp28 and with the N43 of the tetrazole ring interacting with Gly164 (2.8 Å). In molecule B, the thiophene and tetrazole groups have swung up, away from the active site floor and toward the flap. The tetrazole is bound in alternate conformations related by a rotation of 128° about the C35−C37 bond, and stabilized by contacts with residues Leu4, Glu24, Gly29, and Val30 of a neighboring molecule. There is no alternate conformation in molecule A because the tetrazole ring movement is prevented by the OE2 atom of Glu119 of the symmetry-related molecule that interacts through a hydrogen bond with Trp28 O (2.7 Å).

DISCUSSION

The sequence of the IMP-1 metallo β-lactamase from *P. aeruginosa* is 17−37% identical with those of the *B. fragilis*, *B. cereus*, and L1 β-lactamases, and its secondary structure topology is characterized by a central β-sandwich with two α-helices on either side and a binuclear metal center located at one edge of the sandwich (Figure 2). Pairwise superposition of the α-carbon atoms of the IMP-1 and the *B. fragilis* (1ZNB) or the *B. cereus* (1BME) enzymes gives rms deviations of 0.6 Å for both. Except for differences in the flexible flap, there are two other regions that are unique to IMP-1. In the IMP-1 metallo β-lactamase structure, the first β-strand is absent, and the loop between residues 158 and 167 is three residues shorter in the IMP-1 than in the *B. fragilis* or *B. cereus* enzyme. The length of this loop affects the position of the active site Lys161. The absence of three residues in IMP-1 immediately following Lys161 causes the lysine NZ atom to lie 2.0−2.5 Å closer to Zn2. This lysine interacts with the carboxylate of the mercaptocarboxylate inhibitor, and is conserved in all but the *S. maltophilia* metallo β-lactamases where it is a serine (*39*). Given the

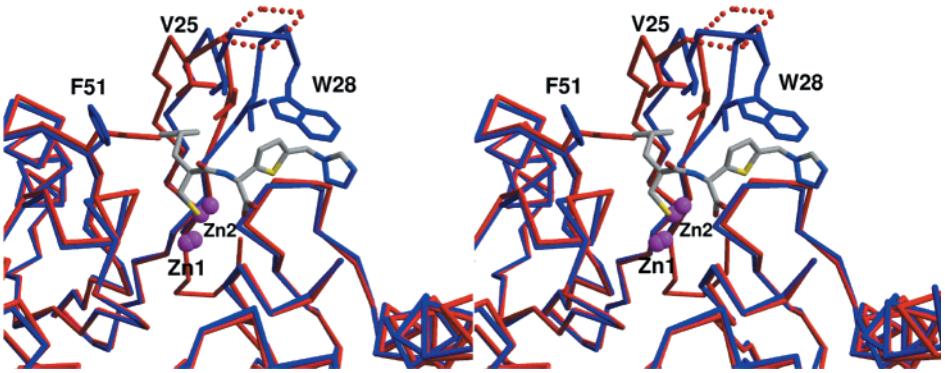

FIGURE 6: Stereoview showing the conformational changes upon inhibitor binding. Superposition of the native, unbound IMP-1 structure (red) and the mercaptocarboxylate complex (blue) (*72*−*74*). The α-carbon atom trace and the side chains of Trp28, Phe51, Val25, and Val31. When the inhibitor is bound, Phe51 rotates 100° around the Cα−Cβ bond to give access to the incoming inhibitor, while Val25 and Val31 are displaced by approximately 2.9 Å compared to the native structure. The lateral movement of the flap widens the S1 hydrophobic pocket. Flap residues G27, W28, and G29 (red dotted line) in the native structure are completely disordered.

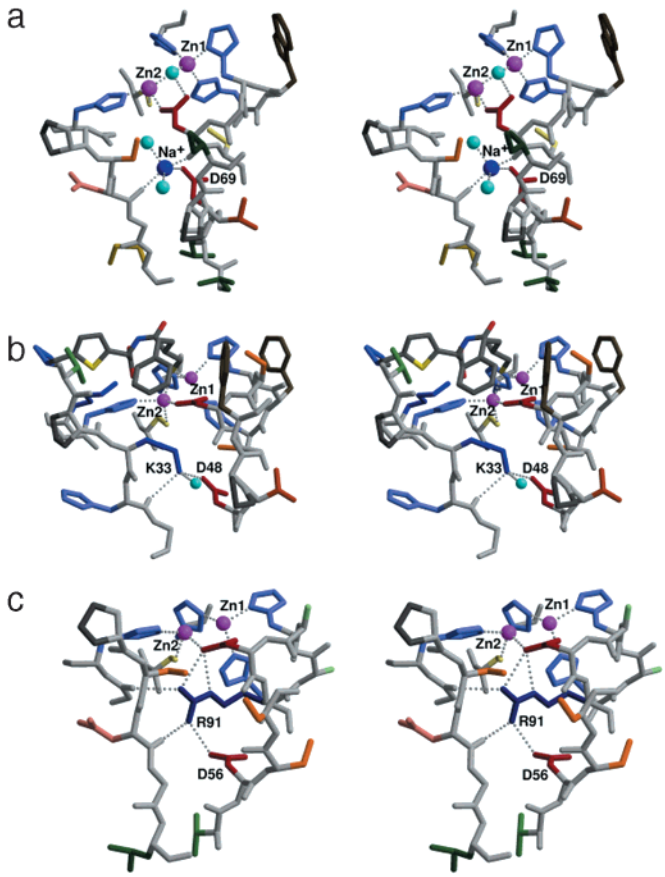

FIGURE 7: Stereoview of the structures of the metallo β-lactamases from *P. aeruginosa*, *B. fragilis*, and *B. cereus* in the vicinity of Asp48 (*72*−*74*). (a) In the *B. fragilis* enzyme, the aspartate interacts with a sodium ion. (b) Asp48 interacts with Lys51 in the IMP-1 enzyme. (c) In the *B. cereus* metallo β-lactamase, the aspartate interacts with an arginine.

similarities among the inhibitor and the substrates, the lysine or the serine may bind to the carboxylate of the β-lactam substrate in a manner similar to that of the mercaptocarboxylate inhibitor.

Asp48 and the equivalent aspartate residues in the *B. fragilis* and *B. cereus* enzymes and the L1 enzyme from *S. maltophilia* have strained main chain conformations, with ϕ and ψ angles for the *B. fragilis* and *B. cereus* enzymes of 81° and 144° and 78° and 150°, respectively, and ϕ and ψ angles of 68° and 157°, respectively, for L1. The conservation of this particular conformation suggests that it is important for the activity of the enzyme, and is consistent with the results from the mutation of this aspartate to an alanine which abolishes the enzymatic activity of the *B. fragilis* enzyme (*46*). The network of interactions that Asp48 establishes near the active site appears to influence the binding affinity of Zn2 depending on the residues with which it interacts. In the IMP-1 enzyme, Asp48 OD interacts electrostatically with Lys33 NZ (2.8 Å); however, in the *B. fragilis* enzyme, instead of a lysine it is a sodium ion (panels a and b of Figure 7), and in the L1 enzyme, it is a water molecule, Wat23, that is bound to the aspartate. The sodium ion in the *B. fragilis* enzyme, the water molecule in the L1 enzyme, and the Lys33 NZ atom in the IMP-1 enzyme occupy equivalent positions and interact with the aspartate. These three metallo β-lactamases, IMP-1, *B. fragilis*, and L1, have two high-affinity metal binding sites. However, in the *B. cereus* enzyme, the equivalent aspartate interacts electrostatically with the side chain of an arginine from a different part of the structure (Figure 7c). The guanidino group atoms of arginine located at position 91 lie close to the binuclear metal center, 4.0−4.4 Å from Zn2, and may interfere electrostatically with binding of the metal as has been pointed out previously (*37*). The arginine is located in the HxHxD**R** sequence motif in which the two histidine residues coordinate Zn1, and the aspartate coordinates Zn2. In the *B. fragilis* or IMP-1 enzyme, a smaller cysteine (Cys104, 1ZNB) or a serine (Ser82, 1DD6), respectively, replaces the arginine at that position and is distant from Zn2. In both the *B. cereus* structure and the *Aeromonas* enzyme, an arginine at this position is associated with a reduced affinity for the second metal binding site. The L1 enzyme with two high-affinity binding sites presents a different arrangement. In the L1 enzyme, which has a lower degree

Table 2: Zinc Ligands[a]

Zn1 (tetrahedral)[b]		Zn2 (tetrahedral)	
H77 NE2	2.2/2.4	D81 OD2	2.1/2.2
H79 ND1	2.2/2.2	C158 SG	2.3/2.4
H139 NE2	2.2/2.2	H197 NE2	2.3/2.4
(I)S	2.2/2.4	(I)S	2.4/2.6

[a] Distances to the metal, in angstroms, are quoted for both molecules in the asymmetric unit. [b] The average ligand−metal−ligand angles for molecule A are 109° for Zn1 and 109° for Zn2; for molecule B, the angles are 109° for Zn1 and 108° for Zn2.

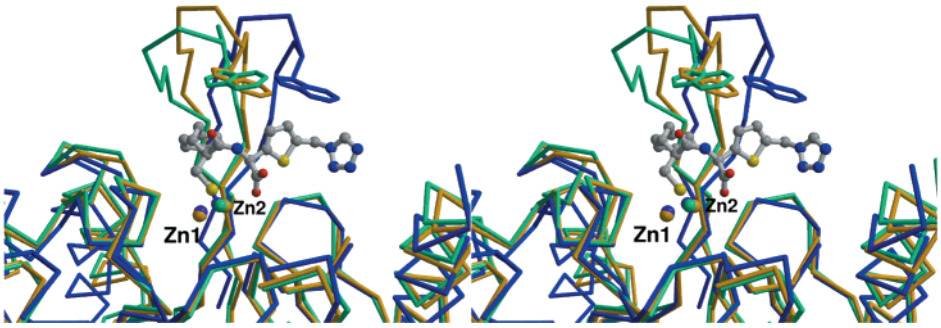

FIGURE 8: Stereoview showing the closed conformation of the flap in the structures of the *B. fragilis* enzyme with MES (gold) (*33*), the *B. fragilis* enzyme with a biphenyl tetrazole inhibitor (green) (*34*), and the *P. aeruginosa* IMP-1 metallo β-lactamase with the mercaptocarboxylate inhibitor (blue) (*72*−*74*). Only the latter inhibitor is shown. The flexible polypeptide chain that forms the flap adopts different conformations to accommodate the inhibitor bound depending on whether the S1 hydrophobic pocket is occupied, as in the IMP-1 complex with the mercaptocarboxylate inhibitor, or not, as in the *B. fragilis* complexes.

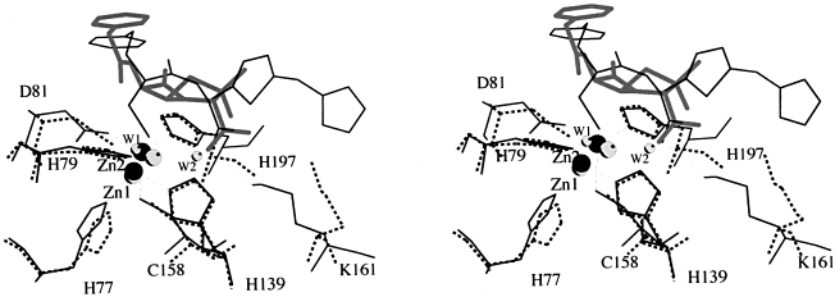

FIGURE 9: Stereoview of the mercaptocarboxylate inhibitor bound to the IMP-1 metallo β-lactamase active site (thin black lines and black spheres) with the docked model of the substrate benzylpenicillin (thick gray line) superimposed such that the phenyl, carboxylate, and carbonyl groups overlap. Also superimposed is the *B. fragilis* (1ZNB) active site residues (dashed lines) and metals and water ligands (light gray spheres). The thiol and carboxylate groups of the inhibitor displaced the shared and apical waters, respectively. Since the binding of the natural substrate is not constrained by the thiol group present in the inhibitor, the substrate's carboxylate may become the fifth ligand to Zn2.

of amino acid sequence identity and more structural differences with respect to the other metallo β-lactamases, a histidine (His89, 1SML) instead of the arginine serves as a ligand to Zn2 (*39*).

The metallo β-lactamases have a wide spectrum substrate specificity, with the exception of the *Aeromonas* enzymes which preferentially hydrolyze carbapenems (*13*, *29*, *68*). Metallo β-lactamases can bind and hydrolyze a variety of substrates, differ in their metal requirement, and constitute a structurally diverse family of proteins that present a challenging opportunity for the design of a wide-spectrum antibiotic. To understand which critical binding interactions need to be established by a potent inhibitor, we have determined the crystal structure of a complex of the IMP-1 metallo β-lactamase from *P. aeruginosa* with a mercaptocarboxylate inhibitor (Figures 2 and 3). The optimal stereochemistry for maximal inhibition of metallo β-lactamase activity and maximal selectivity against other metallo proteases such as angiotensin converting enzyme, ACE, was determined to be *S* and **D**, at C16 and C27, respectively (details of the chemistry and selectivity will be published elsewhere). This mercaptocarboxylate inhibits the IMP-1, *B. fragilis*, and L1 enzymes with IC_{50} values between 100 and 500 nM, being slightly less effective against the L1 enzyme, presumably due to the unique structure of this enzyme as compared with the other metallo β-lactamases. To determine the similarities between the mercaptocarboxylate inhibitor and β-lactam substrates, we used the structure of the complex as a three-dimensional template to manually dock in the active site the substrate benzylpenicillin. The β-lactam was superimposed on the inhibitor such that the carbonyl and carboxylate groups of both molecules overlap (Figure 9). The inhibitor bound in the IMP1 complex resembles the binding mode of the substrate in the model and does not appear to be disturbed by the presence of the thiol group. The phenyl ring of the substrate fits into the hydrophobic pocket at the base of the flap; the carbonyl oxygen is oriented for interaction with Asn167, and the carboxylate interacts with Lys161 with displacement of the apical water coordinated to Zn2 in the native structures. In the inhibitor complex, the carbonyl oxygen is oriented for interactions with Zn1 (5.0 Å) and with Asn167 ND2 (4.1 Å) in the oxyanion hole (*37*), but these rather long distances may be attributed, in part, to the presence of the thiol group in the inhibitor that fixes the position of the carbonyl away from the oxyanion hole. However, it is conceivable that a relatively small displacement of the polypeptide chain in the vicinity of Asn167 could bring the side chain closer to the carbonyl oxygen. In addition, the model of the docked substrate based on the structure of the inhibitor complex implies that after the nucleophilic attack on the carbonyl carbon and the subsequent transition to a tetrahedral carbon (sp^3 hybridization), the distances and directionality of the interaction between the (charged) oxygen atoms with Zn1 and Asn167 could be more favorable. On the basis of the docked model, the substrate uses the same subset of interactions, as does the inhibitor. These three interactions appear to be critical for the specific binding to metallo β-lactamases.

The interaction of the inhibitor's carboxylate with Lys161 highlights the importance of this residue for inhibitor binding

and, possibly, for substrate binding. The proximity of the carboxylate to Zn2 with displacement of the apical water from the Zn2 ligand sphere shows, for the first time, the transition of Zn2 from its native trigonal bipyramid geometry to the tetrahedral coordination in the inhibitor complex (Figure 3). In contrast to the inhibitor complex where the position of the carboxylate is dictated by the presence of the thiol group, it is possible that the carboxylate group of the substrate does become the fifth ligand to Zn2 after displacing the apical water. The potential transition from pentacoordinated to tetracoordinated could be important during catalysis whether the apical water remains as a ligand to Zn2 as part of the Michaelis complex (*37*), or whether the apical water is displaced by the substrate and Zn2 provides electrostatic stabilization of the intermediate (*43*), but from this model, it cannot be determined if the carboxyl group of the substrate and the apical water bind simultaneously in the Michaelis complex or if the water molecule is displaced.

Binding of the mercaptocarboxylate inhibitor to the active site of the IMP-1 metallo β-lactamase triggers the change in the conformation of the flap that leads to closure and interaction with the inhibitor. Binding of the inhibitor requires a rotation about the Cα−Cβ bond of Phe51 (Ile in *B. fragilis* and Trp in *B. cereus*), providing access to the hydrophobic pocket. It also requires that the side chain of Val25 move aside to make the pocket wider, which implies a lateral movement of the flap (Figure 6). In the L1 enzyme structure, where the S1 pocket is formed by residues Tyr11, Val13, Trp17, Leu38, and Met56 (L1 residue numbering, 1SML), it does not appear to be obvious that ligand binding in this pocket could trigger a conformational change as in the IMP-1 or the *B. fragilis* enzyme. However, in the IMP-1−mercaptocarboxylate complex, the closure of the flap entails considerable movement of the polypeptide to bring the indole of Trp28 closer to the active site so that it can interact with the bound inhibitor. With the flap in the closed conformation, the active site becomes a tunnel-shaped cavity with a large opening (Figure 5). Through this opening, the leaving group at C3′ of the β-lactam substrates derived from cephalosporin (*69*) may diffuse into the bulk solvent. The portion of the inhibitor bound near the catalytic center is firmly bound to the enzyme and shows very little difference between the two molecules in the asymmetric unit. The exploitation of possible binding interactions lining the opening of the tunnel may lead to the design of inhibitors with improved binding affinity. The role of the flap for the binding of inhibitors, and the substrates, has been demonstrated in the crystal structures of the mercaptocarboxylate inhibitor complex with IMP-1 presented here, and in the structures of the *B. fragilis* enzymes with MES (*33*) and a biphenyl tetrazole (*34*). Deletion of the flap severely impairs the enzymatic activity by disrupting substrate binding (*70*).

The open, disordered conformation of the flap is found in most native structures of metallo β-lactamases, with the exception of the orthorhombic crystal form of the *B. fragilis* enzyme (*38*) where it is stabilized in the open conformation by crystal lattice contacts. In the L1 enzyme, however, it is not obvious what part of the structure acts as a flap. The crystal structures of inhibitor complexes of the IMP-1 and *B. fragilis* enzymes suggest that the closed conformation of the flap differs depending on whether the S1 hydrophobic pocket near the flap is occupied by the inhibitor (Figure 8). The MES (*33*) and the biphenyl tetrazole inhibitor (*34*) bind in the active site, but neither has groups in the S1 pocket. However, the phenyl group of the mercaptocarboxylate inhibitor bound to the IMP-1 metallo β-lactamase does occupy the pocket. The position of Trp28 gauges the lateral movement of the flap; for example, the position of the α-carbon atom of Trp28 differs by 4.8 Å between the mercaptocarboxylate−IMP-1 and the *B. fragilis* enzyme−MES complexes, and by 6.5 Å between the mercaptocarboxylate−IMP-1 and the *B. fragilis* enzyme−biphenyl tetrazole complexes. These differences are considerably larger than the rms differences in α-carbon atom superposition of ~0.6 Å for pairwise comparisons, and it is not likely to reflect differences in the flap's amino acid sequences between *B. fragilis* and IMP-1 enzymes either. There are 10 residues in the flap: five identical and four conservative replacements; the only possible disrupting replacement is an alanine for a glutamate. The aliphatic side chain of the glutamate forms a side of the hydrophobic pocket and, from its position, is not likely to alter or prevent the motion of the flap.

The crystal structure of the IMP-1 metallo β-lactamase with a potent mercaptocarboxylate inhibitor presented here represents a new mode of binding of a small molecule to a metallo β-lactamase active site, and it shows the critical binding interactions required for a potent inhibitor; it also suggests a mode of substrate binding. The new IMP-1 metallo β-lactamase native structure presented here highlights the structural diversity among this family of proteins. Mercaptocarboxylates have been shown to inhibit IMP-1 and therefore are of great potential in the protection of β-lactam antibiotics against this resistance mechanism and for overcoming bacterial infections caused by metallo β-lactamase-producing organisms.

ACKNOWLEDGMENT

We are grateful to our colleague Dr. Ward W. Smith for critically reading the manuscript and to the reviewer for helpful comments. We are also grateful to Drs. Robert Sweet and Lonny Berman and Mr. Salvatore Sclafani for their assistance in diffraction data acquisition at the National Synchrotron Light Source's X-25 beamline. Diffraction data were collected at the Brookhaven National Laboratory, Biology Department single-crystal facility on beamline X-25 at the National Synchrotron Light Source. This facility is supported by the United States Department of Energy Offices of Health and Environmental Research and Basic Energy Sciences under Contract DE-AC02-98CH10886, by the National Science Foundation, and by National Institutes of Health Grant 1P41 RR12408-01 A1. The HKL package development, used for diffraction data processing, is supported by NIH Grant GM-53163 to the laboratories of Zbyszek Otwinowski (Southwestern Medical Center at Dallas, Dallas, TX) and Wladek Minor (University of Virginia, Charlottesville, VA).

REFERENCES

1. Tenover, F. C., and Hughes, J. M. (1996) *J. Am. Med. Assoc. 275*, 300−304.
2. Domagala, J. M., and Sanchez, J. P. (1997) *Annu. Rep. Med. Chem. 32*, 111−119.

3. Payne, D. J. (1993) *J. Med. Microbiol. 39*, 93−99.
4. Abraham, E. P., and Chain, E. (1940) *Nature 146*, 837−837.
5. Ambler, R. P. (1980) *Philos. Trans. R. Soc. London, Ser. B 289*, 321−331.
6. Jaurin, B., and Grundström, T. (1981) *Proc. Natl. Acad. Sci. U.S.A. 78*, 4897−4901.
7. Houvinen, P., Houvinen, S., and Jacoby, G. A. (1988) *Antimicrob. Agents Chemother. 32*, 134−136.
8. Cartwright, S. J., and Coulson, A. F. W (1980) *Philos. Trans. R. Soc. London, Ser. B 289*, 370−372.
9. Cartwright, S. J., Tan, A. K., and Fink, A. L. (1989) *Biochem. J. 263*, 905−912.
10. Strynadka, N., and James, M. N. G. (1992) *Nature 359*, 700−705.
11. Davies, R. B., and Abraham, E. P. (1974) *Biochem. J. 143*, 129−135.
12. Sabath, L. D., and Abraham, E. P. (1966) *Biochem. J. 98*, 11−13.
13. Felici, A., and Amicosante, G. (1995) *Antimicrob. Agents Chemother. 39*, 192−199.
14. Rasmussen, B. A., Yang, Y. J., Jacobus, N., and Bush, K. (1994) *Antimicrob. Agents Chemother. 38*, 2116−2120.
15. Rasmussen, B. A., Guzman, Y., and Tally, F. P. (1990) *Antimicrob. Agents Chemother. 34*, 1590−1592.
16. Hedberg, M., and Nord, C. E. (1996) *J. Chemother. 8*, 3−16.
17. Thompson, J. S., and Malamy, M. H. (1990) *J. Bacteriol. 172*, 2584−2593.
18. Jouvenot, M., Deschaseaux, M. L., and Royez, M. (1987) *Antimicrob. Agents Chemother. 31*, 300−305.
19. Reid, A. J., Simpson, I. N., Harper, P. B., and Amyes, S. G. B. (1988) *J. Pharm. Pharmacol. 40*, 571−573.
20. Roy, C., Foz, A., and Segura, C. (1983) *J. Antimicrob. Chemother. 12*, 507−510.
21. Senda, K., Arakawa, Y., Nakashima, K., Ito, H., Ichiyama, S., and Shimokata, K. (1996) *Antimicrob. Agents Chemother. 40*, 349−353.
22. Baxter, I. A., and Lambert, P. A. (1994) *FEMS Microbiol. Lett. 122*, 251−256.
23. Saino, Y., Kabayashi, F., Inoue, M., and Mitsuhashi, S. (1982) *Antimicrob. Agents Chemother. 22*, 564−570.
24. Watanabe, M., Iyobe, S., Inoue, M., and Mitsuhashi, S. (1991) *Antimicrob. Agents Chemother. 35*, 147−151.
25. Rossolini, G. M., Franceschini, N., Riccio, M. L., Mercuri, P. S., and Perilli, M. (1998) *Biochem. J. 332*, 145−152.
26. Ito, H., Arakawa, Y., Ohsuka, S., Wacharotayankun, R., Kato, N., and Ohta, M. (1995) *Antimicrob. Agents Chemother. 39*, 824−829.
27. Senda, K., Arakawa, Y., Ichiyama, S., Nakashima, K., Ito, H., Ohsuka, S., Shimokata, K., Kato, N., and Ohta, M. (1996) *J. Clin. Microbiol. 34*, 2909−2913.
28. O'hara, K., Haruta, S., Sawai, T., Tsunoda, M., and Iyobe, S. (1998) *FEMS Microbiol. Lett. 162*, 201−206.
29. Yang, Y. J., and Bush, K. (1996) *FEMS Microbiol. Lett. 137*, 193−200.
30. Payne, D. J., Bateson, J. H., Gasson, B. C., Khushi, T., Proctor, D., and Pearson, S. C. (1997) *FEMS Microbiol. Lett. 157*, 171−175.
31. Bounaga, S., Laws, A. P., Galleni, M., and Page, M. I. (1998) *Biochem. J. 331*, 703−711.
32. Goto, M., Takahashi, T., Yamashita, F., Koreeda, A., Mori, H., and Ohta, M. (1997) *Biol. Pharm. Bull. 20*, 1136−1140.
33. Fitzgerald, P. M. D., Wu, J. K., and Toney, J. H. (1998) *Biochemistry 37*, 6791−6800.
34. Toney, J. H., Fitzgerald, P. M. D., Grover sharma, N., Olson, S. H., and May, W. J. (1998) *Chem. Biol. 5*, 185−196.
35. Carfi, A., Pares, S., Duee, E., Galleni, M., Duez, C., Frère, J.-M., and Dideberg, O. (1995) *EMBO J. 14*, 4914−4921.
36. Carfi, A., Dué, E., Galleni, M., Frère, J.-M., and Dideberg, O. (1998) *Acta Crystallogr. D54*, 313−323.
37. Concha, N. O., Rasmussen, B. A., Bush, K., and Herzberg, O. (1996) *Structure 4*, 823−836.
38. Carfi, A., Duee, E., Paulsoto, R., Galleni, M., Frère, J.-M., and Dideberg, O. (1998) *Acta Crystallogr. D54*, 47−57.
39. Ullah, J. H., Walsh, T. R., Taylor, I. A., Emery, D. C., Verma, C. S., and Gamblin, S. J. (1998) *J. Mol. Biol. 284*, 125−136.
40. Wilcox, D. E. (1996) *Chem. Rev. 96*, 2435−2458.
41. Bicknell, R., and Waley, S. G. (1985) *Biochemistry 24*, 6876−6887.
42. McManus-Munoz, S., and Crowder, M. W. (1999) *Biochemistry 38*, 1547−1553.
43. Wang, Z. G., Fast, W., and Benkovic, S. J. (1998) *J. Am. Chem. Soc. 120*, 10788−10789.
44. Valladares, M. H., Felici, A., Weber, G., Adolph, H. W., and Zeppezauer, M. (1997) *Biochemistry 36*, 11534−11541.
45. Crowder, M. W., Walsh, T. R., Banovic, L., Pettit, M., and Spencer, J. (1998) *Antimicrob. Agents Chemother. 42*, 921−926.
46. Crowder, M. W., Wang, Z. G., Franklin, S. L., Zovinka, E. P., and Benkovic, S. J. (1996) *Biochemistry 35*, 12126−12132.
47. Wang, Z. G., and Benkovic, S. J. (1998) *J. Biol. Chem. 273*, 22402−22408.
48. Baldwin, G. S., Galdes, A., Hill, A. O., Smith, B. E., Waley, S. G., and Abraham, E. P. (1978) *Biochem. J. 175*, 441−447.
49. Fabiane, S. M., Soshi, M. K., Wan, T., Payne, D. J., Bateson, J. H., Mitchell, T., and Sutton, B. J. (1998) *Biochemistry 37*, 12404−12411.
50. Lauretti, L., Riccio, M. L., Mazzariol, A., Cornaglia, G., Amicosante, G., Fontana, R., and Rossolini, G. M. (1999) *Antimicrob. Agents Chemother. 43*, 1584−1590.
51. Arakawa, Y., Murakami, M., Suzuki, K., Ito, H., Wacharotayankun, R., Ohsuka, S., Kato, N., and Ohta, M. (1995) *Antimicrob. Agents Chemother. 39*, 1612−1615.
52. Hirakata, Y., Izumikawa, K., Yamaguchi, T., Takemura, H., Tanaka, H., Yoshida, R., Matsuda, J., Nakano, M., Tomono, K., Maesaki, S., Kaku, M., and Yamada, Y. (1998) *Antimicrob. Agents Chemother. 42*, 2006−2011.
53. Laraki, N., Franceschini, N., Rossolini, G. M., Santucci, P., Meunier, C., De Pauw, E., Amicosante, G., Frère, J.-M., and Galleni, M. (1999) *Antimicrob. Agents Chemother. 43*, 902−906.
54. Kabsch, W. (1988) *J. Appl. Crystallogr. 21*, 916−924.
55. Otwinowski, Z., and Minor, W. (1997) *Methods Enzymol. 276*, 307−326.
56. Navaza, J. (1994) *Methods Enzymol. 276*, 581−594.
57. Collaborative Computational Project No. 4 (1994) *Acta Crystallogr. D50*, 760−763.
58. Brünger, A. T. (1992) *X-plor version 3.1: A system for X-ray crystallography and NMR*, Yale University Press, New Haven, CT.
59. Brünger, A. T., Adams, P. D., Clore, M., DeLano, W. L., Gros, P., Grosse-Kunstelev, R. W., Jian, J.-S., Kruszewski, J., Nilges, M., Pannu, N. S., Read, R. J., Rice, L. M., Simonson, T., and Warren, G. L. (1998) *Acta Crystallogr. D54*, 905−921.
60. Jones, T. A., Zou, J.-Y., Cowan, S. W., and Kjelgaard, M. (1991) *Acta Crystallogr. A47*, 110−119.
61. Kleywegt, G. J. (1995) *CCP4/ESF-EACBM Newsletter on Protein Crystallography 31 June*, pp 45−50.
62. Pannu, N. S., and Read, R. J. (1996) *Acta Crystallogr. A52*, 659−688.
63. Read, R. J. (1986) *Acta Crystallogr. A42*, 140−149.
64. Brünger, A. T. (1992) *Nature 355*, 472−475.
65. Jiang, J.-S., and Brünger, A. T. (1994) *J. Mol. Biol. 243*, 100−115.
66. Payne, D. J., Cramp, R., Winstanley, D., and Knowles, D. (1994) *Antimicrob. Agents Chemother. 38*, 767−772.
67. Engh, R. A., and Huber, R. (1991) *Acta Crystallogr. A47*, 392−400.
68. Walsh, T. R., Gamblin, S., Emery, D. C., Macgowan, A. P., and Bennett, P. M. (1996) *J. Antimicrob. Chemother. 37*, 423−431.
69. Buckwell, S. C., Page, M. I., Longridge, J. L., and Waley, S. G. (1988) *J. Chem. Soc., Perkin Trans. 2*, 1823−1827.

70. Yang, Y. J., Keeney, D., Tang, X., Canfield, N., and Rasmussen, B. A. (1999) *J. Biol. Chem. 274*, 15706−15711.
71. Kabsch, W., and Sander, C. (1983) *Biopolymers 22*, 2577−2637.
72. Kraulis, P. J. (1991) *J. Appl. Crystallogr. 24*, 946−950.
73. Bacon, D. J., and Anderson, W. F. (1988) *J. Mol. Graphics 6*, 219−220.
74. Merritt, E. A., and Murphy, M. E. P. (1994) *Acta Crystallogr. D50*, 869−873.
75. Hodel, A., Kim, S.-H., and Brunger, A. T. (1992) *Acta Crystallogr. A48*, 851−858.
76. Wallace, A. C., Laskowski, R. A., and Thornton, J. M. (1995) *Protein Eng. 8*, 127−134.
77. Nicholls, A., Sharp, K. A., and Honig, B. (1991) *Proteins 11*, 281−296.

BI992569M